Pharmacology, Biochemistry and Behavior 90 (2008) 664–675

Contents lists available at ScienceDirect

Pharmacology, Biochemistry and Behavior

journal homepage: www.elsevier.com/locate/pharmbiochembeh

Role of p38 mitogen activated protein kinase in a model of osteosarcoma-induced pain

Camilla I. Svensson [a,*,1], Satyanarayana Medicherla [d,1,2], Shelle Malkmus [a], Yebin Jiang [c], Jing Y. Ma [d], Irena Kerr [d], Josue Brainin-Mattos [a], Harry C. Powell [b], Z. David Luo [a,3], Sarvajit Chakravarty [d], Sundeep Dugar [d], Linda S. Higgins [d], Andrew A. Protter [d], Tony L. Yaksh [a]

[a] Department of Anesthesiology, University of California, San Diego, La Jolla, CA, United States
[b] Department of Pathology, University of California, San Diego, La Jolla, CA, United States
[c] Department of Radiology, University of Michigan Medical School, Ann Arbor, MI, United States
[d] Scios Inc., Fremont, CA, United States

ARTICLE INFO

Article history:
Received 17 November 2007
Received in revised form 20 May 2008
Accepted 22 May 2008
Available online 3 June 2008

Keywords:
Allodynia
Bone cancer
Dorsal root ganglion
p38 MAPK
Osteosarcoma
Pain
SCIO-469
Spinal cord

ABSTRACT

The focus of this work was to examine the potential role of p38 mitogen activated protein kinase (p38) in a mouse model of bone cancer (osteosarcoma) pain. To generate osteosarcoma and sham animals, osteosarcoma cells or medium were injected into the medullary canal of the femur. Initially, ipsilateral tactile allodynia was observed in both groups, but by 12 days post-surgery, thresholds in the sham group returned towards baseline while hypersensitivity in the osteosarcoma group lasted throughout the study. An increase in phosphorylated p38 was detected by western blotting in dorsal root ganglia (DRG) and spinal cord day 14 after surgery. Immunohistochemistry showed that p38 was phosphorylated in DRG and spinal dorsal horn neurons at this time point. Two doses of a selective p38 inhibitor, SCIO-469, were administered in the chow starting 5 days post-surgery and continued throughout the study. Treatment with SCIO-469 led to a decrease in osteosarcoma-induced clinical score but had no effect on the allodynia. Bone erosion and tumor growth were also examined but no significant reduction of bone erosion or tumor growth was observed in the SCIO-469 treated mice. These data suggest that the p38 signaling pathway does not play a major role in bone cancer-mediated pain.

1. Introduction

Seventy-five to ninety percent of patients with advanced cancer experience significant and debilitating pain (Portenoy et al., 1999). Cancers that lead to destruction of bone are particularly painful and the pain is difficult to treat. Malignant bone tumors can occur in patients as primary tumors but bone is also the most common site for metastasis in a variety of cancers, including breast, prostate, melanoma and lung cancer (Yoneda, 1998; Coleman, 2001). Most of the clinical problems associated with skeletal tumors are a result of the cancer-induced alteration in bone turnover. Severe pain, pathological fractures, nerve compression syndromes and hypocalcaemia are among the many problems that patients with bone cancer may endure. Although pain is one of the most frequent and disruptive symptoms in these patients, the mechanism responsible for the induction and maintenance of bone cancer pain is not clearly understood.

In general, persistent pain is thought to depend on the expression and release of factors at the injury site that sensitize the peripheral nerve and the subsequent sensitization at the spinal level, which leads to a potent facilitation of pain processing (Woolf and Salter, 2000). Previous work has shown that there are distinct neurochemical differences in primary afferent neurons and in the spinal cord in inflammatory and neuropathic pain states (Scholz and Woolf, 2002). Although bone cancer is associated with both inflammation and nerve-injury, studies have demonstrated that bone cancer pain is not "just" the sum of these two mechanisms; it is more likely driven by a unique neurochemical state (Honore et al., 2000). In addition to ongoing inflammation and nerve damage, it is likely that the mechanism by which malignant bone disease causes pain is mediated also by tumor growth and the associated bone destruction (Luger et al., 2005). This multifactorial input may be part of the reason for the difficulty to adequately treat bone cancer pain. From this point of view, p38, a member of the mitogen activated protein kinase (MAPK) family is interesting as it is involved in a wide range of cellular functions and often has been implicated in pathological conditions. p38 is a serine/threonine kinase that transduces extracellular stimuli into intracellular post-

* Corresponding author. Department of Anesthesiology, University of California, San Diego, 9500 Gilman Drive, La Jolla, CA, 92093-0818, United States. Tel.: +1 619 543 6197; fax: +1 619 543 6070.
E-mail address: csvensson@ucsd.edu (C.I. Svensson).
[1] Camilla I. Svensson and Satyanarayana Medicherla contributed equally to this work.
[2] Present address: Schering-Plough Biopharma, 901 California Avenue, Palo Alto, CA, United States.
[3] Present address: Department of Anesthesiology, University of California, Irvine, Irvine, United States.

0091-3057/$ – see front matter © 2008 Elsevier Inc. All rights reserved.
doi:10.1016/j.pbb.2008.05.016

translational and transcriptional responses (Widmann et al., 1999; Ono and Han, 2000). It has been demonstrated that p38 plays an important role in pain processing by regulating peripheral and spinal neuronal sensitization initiated by inflammatory (Ji et al., 2002; Svensson et al., 2003b) and neuropathic (Jin et al., 2003; Schafers et al., 2003; Obata et al., 2004; Tsuda et al., 2004) stimuli. In addition, p38 is involved in the regulation of osteoclastogenesis (Matsumoto et al., 2000a,b; Lee et al., 2002; Zwerina et al., 2006b) and formation of bone metastasis (Matsumoto et al., 2000a; Selvamurugan et al., 2002; Suarez-Cuervo et al., 2004; Zwerina et al., 2006b).

In light of the multiple mechanisms through which p38 may contribute to bone cancer pain, we examined the role of p38 in an in vivo model of bone cancer. In this model, syngeneic osteolytic sarcoma cells are injected and confined to the marrow space of the mouse femur (Schwei et al., 1999). Behavioral and anatomical studies have shown that these mice develop a hypersensitivity to an otherwise non-noxious (non-painful) stimuli, referred to as allodynia. This allodynia is associated with activation of peripheral neurons as well as changes in the dorsal horn of the spinal cord such as hypertrophy of glia cells and alteration of expression of neurotransmitters(Schwei et al., 1999). There is an increase in tumor burden and osteoclast-associated bone resorption in the tumor-invaded bone in this model, which is believed to contribute to stimulation of peripheral nociceptors. We found that after injection of tumor cells there is a unique pattern of p38 activation in DRGs and in the lumbar spinal cord on the side corresponding to the tumor-bearing femur. Subsequently, we tested the effectiveness of SCIO-469, a selective p38 inhibitor, in attenuating allodynia, bone destruction and tumor growth.

2. Materials and methods

2.1. Animals

All experiments were carried out according to protocols approved by the Institutional Animal Care Committee of University of California, San Diego. Male mice (20–25 g, C3H/HeJ, Jackson Labs, Bar Harbor, Maine) were housed in accordance with the National Institute of Health guidelines in micro-isolator filter cages and maintained on a 12-h light/dark cycle with free access to food and water.

2.2. Culture and injection of tumor cells

The murine bone cancer model was performed as previously described by Schwei et al., 1999. In brief, mice were anesthetized with xylazine/ketamine mixture (10 mg/kg xylazine, 100 mg/kg ketamine) and the lateral femur was prepared for surgery. A skin incision was made parallel to the femur to expose the patella, which was dislocated medially to expose the lateral chondyle. A small hole was drilled to access the medullary space for cell injection. Each animal was slowly injected with approximately 10^3 or 10^5 tumor cells (NCTC clone 2472 osteolytic sarcoma cells, American Type Culture Collection, Rockville, MD, Catalog # CCL-11) delivered through a 30 gauge needle in 20 µl of α minimum essential media (αMEM) containing 1% bovine serum albumin (BSA). Sham mice were injected with 20 µl of cell free αMEM containing 1% BSA. A dental amalgam plug was used to seal the injection site and confine the cancer cells to the medullary cavity. The wound site was irrigated with sterile water and closed using 3–0 silk. Sutures were removed 5–7 days post-surgery to facilitate behavioral testing.

2.3. Dosing preparation

To assess the effect of p38 inhibition on pain related behaviors and bone destruction, the p38 inhibitor SCIO-469 (Scios Inc. Sunnyvale) was blended into powdered chow (Lab Diet-5015, Dean's Animal Feeds, San Carlos, CA) at doses of 1.3 mg/g or 4 mg/g of chow. Based on data indicating that the typical daily chow consumption in this strain and age of mouse is approximately 3 g/day, the target doses were 200 mg/kg/day (low dose) and 600 mg/kg/day (high dose). Pilot pharmacokinetic studies were undertaken to determine if drug delivered in powdered chow produced appropriate plasma levels. In these studies, groups of mice (n=5/treatment) were given access to powdered chow with the respective “200” and “600” mg/kg doses of SCIO-469. Animals were sacrificed at mid-day after 2 or 14 days of chow exposure. Plasma drug concentrations of 5±1 µM and 15±3 µM were observed in the 200 and 600 mg/kg groups, respectively, at day 2 and 7.5±2.5 µM and 29±7 µM, respectively, after 14 days of feeding. During the course of the study, body weight and food consumption were assessed daily. As mice were housed in groups of 3, the measured food consumption was expressed as total measured food consumed daily divided by 3. As will be discussed below, food intake was not affected by the presence of drug in the diet. These preliminary observations indicate significant dose-dependent blood levels during the course of the study and around the time of testing.

2.4. Treatment groups

Table 1 outlines the 5 groups included in this study. Sham animals were injected with cell culture media and received powered food only. Animals in the tumor-bearing groups were assigned to receive either 10^3 or 10^5 cells. Based on the outcome of the initial study, the animals injected with 10^5 cells were then assigned to a control group given powdered food only, or to a treatment group given either low dose or high dose SIOS 469 starting on post-surgery day 5.

Table 1
Groups of sham and osteosarcoma mice with treatment, number and experimental timeline for the four experiments included in this study

Study	No.of cancer cells	Group	Drug treatment	No.of mice	Test day [ambulation, allodynia]	Radiograph day	Sacrifice day
1	Media only	Sham	Food only	9	0, 5, 15	5, 14	15
1	10^3	Osteosarcoma No treatment	Food only	12	0, 5, 15	5, 14	15
2	Media only	Sham	Food only	8	0, 4, 5, 8, 10, 12, 15, 16	5, 13,16	16
2	10^5	Osteosarcoma No treatment	Food only	8	0, 4, 5, 8, 10, 12, 15, 16	5, 13,16	16
3	Media only	Sham	Food only	12	0, 5, 16	5, 13,16	16
3	10^5	Osteosarcoma No treatment	Food only	8	0, 5, 16	5, 13,16	16
3	10^5	Osteosarcoma Low dose	SCIO-469 200 mg/kg/day	12	0, 5, 16	5, 13,16	16
3	10^5	Osteosarcoma High dose	SCIO-469 600 mg/kg/day	12	0, 5, 16	5, 13,16	16
4	10^5	P38 phosphorolation	Food only	4	n/a	n/a	2
4	10^5	P38 phosphorolation	Food only	4	n/a	n/a	7
4	10^5	P38 phosphorolation	Food only	4	n/a	n/a	14

In a separate study, animals injected with 10^5 osteosarcoma cells were sacrificed on days 2, 7 and 14 for examination of phosphorylation of p38 in the spinal cord and dorsal root ganglia by western blotting and day 14 for immunohistochemical studies. These animals were not subjected to behavioral testing.

2.5. Behavioral analysis

To monitor the general health of the mice, body weights were recorded every day and animals were monitored for side effects such as ataxia, illness and lethargy. Visual observation of the animals in the cage was first done to observe the status of spontaneous behavior, posture and hair coat. Reluctance to move, hunched posture, piloerection and tacky hair coat due to lack of grooming were indications of illness and lethargy. Animals were then removed from the cage, weighed, and placed on a surface for observation of normal symmetry of ambulation. Bright, alert and responsive behavior, symmetric ambulation and the absence of weight loss indicated that the animals were healthy and that tumor-bearing animals were not in a state of cachexia. These and additional clinical behavioral parameters were scored at intervals prior to and following surgical injection of cells.

2.5.1. Clinical score

Assessment of spontaneous pain was based on vocalization, guarding (avoiding hind limb movement) and ambulation and denoted "clinical score". The animal was placed on a paper covered lab bench surface and allowed to explore. Spontaneous vocalization or vocalization evoked during clinical observations was recorded. Asymmetric ambulation or favoring of one hind limb with posture or a hunched back during ambulation or while still was recorded. Guarding behaviors in which the animal avoided movement of the affected hind limb, as seen by failure to extend the hind limb when the back legs were raised from the surface by lifting the tail was observed. These three clinical parameters were scored on a scale of 0–3 as follows. animals were scored on a scale of 0–3 as follows: (0) Absence of deficit, normal behavior (baseline), (1) slight deficit, noticeable change in parameter being evaluated, 5–25% change from baseline or displays occasional episodes; (2) moderate deficit, significant difference apparent upon first observations, 26–50% change from baseline, or displays frequent episodes; (3) marked or severe deficit, debilitating, >50% change from baseline, or displays frequently repeated occurrences of the observation. Total scores for the three parameters were added and then divided by three to obtain the clinical score. The clinical score was assessed prior to surgery, at intervals post-surgery and on the day of, or one day prior to, sacrifice. To permit statistical analysis of these data, ratios of post to pre were calculated. These ratios were determined by dividing the baseline values by the final study day. In order to calculate the ratios for the clinical scores, in which the baseline was zero, scores were inverted (i.e., 0=3, 1=2, 2=1, 3=0).

2.5.2. Tactile threshold

The tactile threshold model was used to assess tactile allodynia, an increased sensitivity to an otherwise non-noxious mechanical stimulus. The mice were placed in a clear plastic, wire mesh-bottomed cage, divided into individual compartments and allowed to acclimate prior to testing. Baseline withdrawal thresholds were assessed with calibrated von Frey filaments (Stoelting, Wood Dale, IL.) having buckling forces between 0.036 and 2.34 g prior to surgery and SCIO-469 treatment. Each filament was pressed perpendicularly against the mid hind paw, avoiding the tori, with sufficient force to cause slight bending, and held for approximately 4 s. A positive response was noted if the paw is sharply withdrawn. Testing began with the 0.4 g filament and proceeded according to the up-down method described by Chaplan et al. (1994). The 50% probability withdrawal threshold was determined. Tactile allodynia was assessed prior to surgery, at intervals post-surgery and on the day of, or one day prior to sacrifice. To normalize baseline values and compare the degree of allodynia resulting from injection of 10^3 or 10^5 cells, the ratio of the baseline allodynia score to the final allodynia score was obtained for each animal and the mean values for both cell concentrations are presented.

2.6. Quantification of bone destruction, osteolysis

2.6.1. Radiographic analysis

On day 5 and 13 post-surgery, and the day of, or one day prior to necropsy, animals were anesthetized (ketamine, 100 mg/kg and xylazine, 10 mg/kg) and radiographs of the affected hind limb were obtained. Images were captured on Kodak Portal Pack film (Kodak, Rochester, NY) using a Faxitron Specimen Radiography System (Faxitron X-ray Corporation, Wheeling, IL). Radiographs were evaluated by three blinded independent observers. The entire femur from the head of the femur to the lateral condoyle was considered in the evaluations. The extent of bone osteolysis was quantified on a scale of one to three. A score of (0) was given in normal bone, (1) if there was mild or up to 25% lysis of the affected bone, (2) if there was apparent or up to 50% lysis of the affected bone or (3) if there was greater than 50% lysis or complete fracture of the bone. On the day of sacrifice, femurs were harvested and placed in either 10% formalin for histology or 70% ethanol for μ-CT.

2.6.2. Histomorphological analysis and quantification of tumor growth

Femurs were decalcified, paraffin embedded longitudinally, sections (5 μm) were cut in frontal plane and stained with hematoxylin and eosin (H&E). Femurs were imaged using a microscope equipped with a digital camera and image-capture software (Image Pro Plus 4.5 software, Media Cybernatics Inc, Silver Spring, MD). The total area of intramedullary space and the intramedullary space occupied with tumor mass was measured and the results expressed as percentage of intramedullary space occupied by tumor. The number of osteoclasts was counted at the bone/marrow (tumor) interface along the whole length of the femur using an inverted microscope (Nikon TS100) and camera (Nikon CCD 5.1 megapixels, Nikon Instruments Inc, USA). The presence of osteoclasts was detected by tartrate-resistant acid phosphatase (TRAP) staining (Sigma; St. Louis, MO). Quantification of active osteoclasts, defined as multinucleated TRAP-positive cells, was performed by a blinded examiner counting total number of osteoclasts in contact with the bone surface along the whole length of the femur.

2.6.3. Micro-computed tomography (μ-CT) imaging

Femurs were scanned in a micro-computed tomography (micro-CT) system in order to obtain a three-dimensional trabecular microstructure. μ-CT imaging acquisition and quantitative analysis of bone structure were conducted as described by Jiang et al. (2002) and Takeshita et al. (2002). In brief, from the original image analyses, we analyzed a subvolume containing the cortical bone and trabecular bone in the epiphysis and metaphysis of the femur. The volumetric data were divided by predetermined thresholds into binary data sets, and the bone tissue was segmented from non-bone in the gray-value images with a fixed thresholding procedure for all samples. Parameters held constant included the filter width (Parfitt et al., 1983; Jiang et al., 2002), the filter support (2.0), and the threshold (27.5% of maximal possible gray value). Three-dimensional trabecular structural parameters were measured without stereological model assumptions, as described previously.

Total bone volume per tissue volume (BV/TV), connectivity density (a measure for the number of trabeculae per unit volume) and cortical thickness (expressed as the average thickness of the 3D cortex across the inner and outer cortical surfaces of the specimen)were assessed as described in our earlier communications (Jiang et al., 2000; Medicherla et al., 2006). In brief, mineralized bone was separated from bone marrow with a 3-D segmentation algorithm. The algorithm for separating mineralized bone from bone marrow was based on an analysis of the steepest gradient calculated from a continuous polynomial fit least-squares approximation of the originally discrete CT volume to find

digital edges. Bone volume was calculated using tetrahedrons corresponding to the enclosed volume of the triangulated surface. Total volume was the volume of the sample that was examined. A normalized index, bone volume/trabecular volume, was used to compare samples of varying size. Bone structural thickness was estimated computationally by using the method of maximal spheres and then calculating the average thickness of all bone voxels (volume pixels). Bone structural separation was calculated with the same procedure as thickness, but the voxels representing non-bone parts were filled with maximal spheres.

2.7. Western blot analysis of MAPK phosphorylation in DRGs and spinal cord

Before sacrifice, mice were deeply anesthetized (Beuthanasia-D solution, Sigma, 0.1 ml intraperitoneal), and, after decapitation, the spinal cords (L1–L6) and DRGs (L2–L5) were collected by laminectomy. The lumbar part of the spinal cord was split into contralateral and ipsilateral halves and immediately homogenized in extraction buffer (50 mM Tris buffer, pH 8.0, containing 0.5% Triton X-100, 150 mM NaCl, 1 mM EDTA, protease inhibitor cocktail [Sigma] and phosphatase inhibitor cocktail I and II [Sigma]) by sonication. After centrifugation (15 min at 14,000 rpm), the supernatant was collected and the protein concentration measured using BCA protein assay (Pierce, Thermo Scientific, Rockford, IL). The tissue extracts (50 μg/well) were subjected to denaturing NuPAGE 4–12% Bis–Tris gel electrophoresis and then transferred to nitrocellulose membranes (Invitrogen, Carlsbad, CA, USA). After blocking non-specific binding sites with 5% low-fat milk in Tris-based buffer (50 mM Tris-Cl, 6 mM NaCl) containing 0.1% Tween 20 for 1 h at room temperature, the membranes were incubated with antibodies overnight at 4 °C. After washing, the antibody–protein complexes were probed with appropriate secondary antibodies labeled with horseradish peroxidase for 1 h at room temperature and detected with chemiluminescent reagents (Super-Signal; Pierce, Thermo Scientific, Rockford, IL, USA). The nitrocellulose membranes were stripped with a Re-Blot western blot recycling kit (Chemicon, Temecula, CA, USA) and reblotted with two different antibodies. The antibodies used in this study were: phosphorylated (P) p38, total p38 (1:1000; Cell Signaling Technology, Beverly, MA, USA) and β-actin (1:25,000; Sigma) and the membranes probed with antibodies in that order. The intensity of immunoreactive bands was quantified using ImageQuant software (Molecular Dynamics, Sunnyvale, CA, USA). Immunopositive bands were normalized relative to β-actin and expressed as % change from contralateral sample.

2.8. Immunohistochemistry

Animals were deeply anesthetized (Beuthanasia-D solution, 0.1 ml intraperitoneal) and perfused intracardially with heparinized saline followed by freshly prepared 4% paraformaldehyde in 0.1 m phosphate-buffered saline (pH 7.4; Sigma). The lumbar spinal cord and DRGs (L3–L5) were removed, post-fixed in the same fixative for 6 h and transferred to phosphate-buffered saline containing 20% sucrose for 24 h and then 30% sucrose for 48 h. The lumbar segments L1–L6 were dissected, frozen and transverse sections (10 μm) were cut with and mounted on silane-covered glass slides. Non-specific binding was blocked by incubation in 5% normal goat serum in phosphate-buffered saline with 0.2% Triton X-100 followed by incubation with primary p38 antibody (generated in rabbit, 1:500; Cell Signaling Technology) overnight at 4 °C under gentle agitation. Binding sites were visualized with anti-rabbit IgG antibodies conjugated with Alexa-488 (1:250, Invitrogen). Sections were counterstained with marker for neurons (Neuronal N, 1:1000; Chemicon) following the same over night procedure. Binding sites were visualized with anti-mouse IgG antibody conjugated with Alexa-594 (1:250, Invitorgen, USA). Non-specific staining was determined by excluding the primary antibodies. Images were captured using a deconvolution microscopy system (Nikon, Melville, NY, USA) operated by Lasersharp 2000 software (Biorad, Hemel Hemstead, UK).

2.9. Serum concentrations of SCIO 469

On the day of sacrifice the animals were anesthetized (ketamine, 100 mg/kg and xylazine, 10 mg/kg) and blood samples collected by cardiac puncture. Approximately 0.1 ml of plasma was prepared from each mouse, frozen on dry ice, and then stored at −80 °C until analysis. SCIO-469 in plasma was measured by reverse-phase LC/MS/MS. Briefly, SCIO-469 and the internal standard NPC-31467 were extracted from rat plasma by protein precipitation. The extract was injected onto a Pursuit diphenyl column (Varian, Inc., Palo Alto, CA) with a gradient between 0.2% acetic acid in water and 0.2% acetic acid in methanol. Analysis was on an ABI-Sciex API 4000 mass spectrometer (Applied Biosystems, Inc., Foster City, CA) operated in the positive ion TurboIonSpray mode.

2.10. Statistical analysis

Analyses were carried out using Prism statistical software (GraphPad Software Inc. San Diego, CA). Analysis differences reaching a $P<0.05$ level of significance was defined as statistically significant.

2.10.1. Body weights and food consumption

For statistical analysis, the mean body weights, and food consumption were calculated over 4 intervals; day −4 to −1 (pre-osteosarcoma); day 0–4 (post-osteosarcoma/pre-drug); day 5–12 (early post-treatment) and 13–15 (late post-treatment). Repeated measures ANOVA of each treatment group were undertaken with *post hoc* comparisons between intervals. As mice were housed in groups of 3, the data for food consumption presents the total measured food consumption divided by 3.

2.10.2. Behavioral assessment and osteolysis

Data are presented as the ratio of presurgery score to the day 14/16 score. One-way ANOVAs across treatment group were undertaken with *post hoc* comparisons between treatments.

2.10.3. Western blot

For assessment of protein levels by Western blotting 4 animals were included in each group. Differences between groups were compared with one-way ANOVA and Bonferroni *post hoc* test.

3. Results

3.1. Tactile allodynia and clinical score

All groups, including the sham group, displayed tactile allodynia and modest impairment in the clinical score 5 days post-surgery (Fig. 1a, b). By day 15/16, however, tactile thresholds in sham operated animals had returned towards baseline levels, whereas the animals receiving tumor cells displayed a persistent impairment which was related to the number of tumor cells injected. Thus, animals receiving 10^3 cells displayed a modest tactile allodynia with no impairment of ambulation while the animals receiving 10^5 cells displayed more prominent allodynia and impairment of ambulation (Fig. 1a, b). Though there was no statistical difference between paw withdrawal thresholds at any time, normalization of the degree of allodynia as determined by calculating the individual ratio of day 0 vs day 15/16 for each mouse, revealed a statistical significant allodynia in the group injected with 10^5 osteosarcoma cells into the femur (Fig. 1c). Calculation of the ratio for the clinical score showed that impairment of the ambulation was again significant only in the 10^5 cell group (Fig. 1d). Based on these results, 10^5 cells were injected into the femur in the subsequent studies.

In a separate study, mice were injected with 10^5 osteosarcoma cells, or media, to the medullary space and the response to tactile stimulation recorded day 4, 5, 8, 10, 12, 15 and 16. Also in this study did both the osteosarcoma and the sham group display tactile allodynia

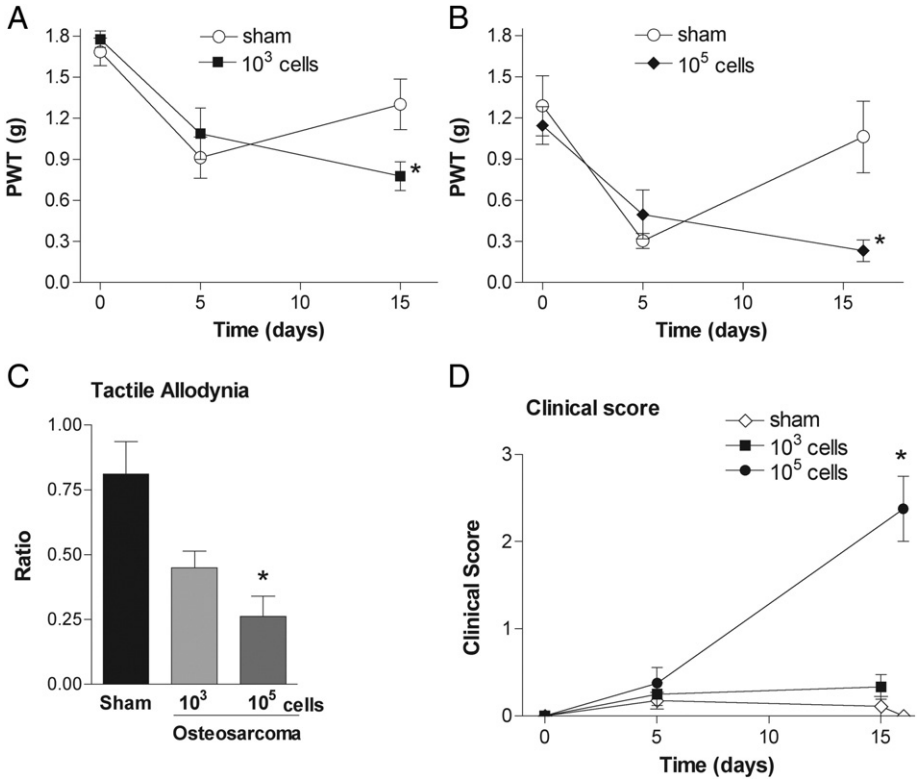

Fig. 1. Allodynia and clinical score after injection of osteosarcoma cells to the femur. Tactile thresholds over time measured by von Frey filaments in the groups receiving (A) 10^3 and (B) 10^5 cells. (C) To normalize baseline values and compare the degree of allodynia resulting from injection of 10^3 or 10^5 cells, the ratio of the baseline allodynia score to the final allodynia score (day 15–16) was calculated for each animal and the mean values for sham and osteosarcoma groups presented. (D) The behavioral impairment was scored on a scale of 0–3, where 0 represents baseline (normal) behavior and 3 represents severe dysfunction as characterized by favoring (limping), vocalization and guarding of the injected hind paw. Each time point and bar represents mean±SEM, n=8–17 mice per group.

initially, but by day 12 the tactile threshold in the sham group was returning towards baseline while the osteosarcoma group displayed allodynia throughout the study (Fig. 2).

3.2. Temporal activation of p38 in dorsal root ganglia and spinal cord in sham and osteosarcoma mice

To examine the temporal profile of p38 phosphorylation during the development of osteosarcoma-induced allodynia and bone destruction, DRGs (L3–L5) and spinal cords (L1–L6) were collected from sham and osteosarcoma mice (injected with 10^5 tumor cells) 2, 7 and 14 days post-surgery. Interestingly, both sham and osteosarcoma mice showed an initial (day 2) increase in p38 phosphorylation in ipsilateral DRG (osteosarcoma, 282±33%; sham, 326±59%, $P<0.05$, Fig. 3a, c) and spinal (osteosarcoma, 191±36; sham, 184±19%, $P<0.05$, Fig. 3b, d) samples, as compared to the contralateral side. Seven days after surgery, no difference in p38 phosphorylation was observed between ipsilateral and contralateral tissue from the sham or the osteosarcoma DRGs or spinal cord. In contrast, 14 days after surgery there was a marked difference between the sham and osteosarcoma group. p38 phosphorylation was elevated in ipsilateral DRGs from osteosarcoma mice, as compared to ipsilateral DRGs from sham mice (478±17% vs 102±40%, $P<0.05$). There was also a significant increase in p38 phosphorylation ipsilateral to the tumor cell injection in the spinal cord compared to sham mice, 209±18% vs 108±13%, $P<0.05$).

3.3. Cellular distribution of p38 activation in dorsal root ganglia and spinal dorsal horn neurons

In studies of inflammation or nerve-injury induced pain, it has been demonstrated that p38 is phosphorylated in DRG neurons and spinal microglia, and to some extent in subpopulations of dorsal horn neurons (Ji et al., 2002; Schafers et al., 2003; Svensson et al., 2003a,b). P-p38 immunohistochemistry was undertaken to determine the cellular distribution of p38 activation in DRGs and spinal cord at a time point where the osteosarcoma is well established and the mice display tactile allodynia dissociated from pain behavior in the sham group. For this purpose, DRGs and spinal cords were harvested 14 days after tumor cell placement. P-p38 immunoreactivity was observed in ipsilateral small and medium sized neurons in L3–L5 dorsal root ganglia (Fig. 4). P-p38 immunoreactivity was strong in the nuclei of

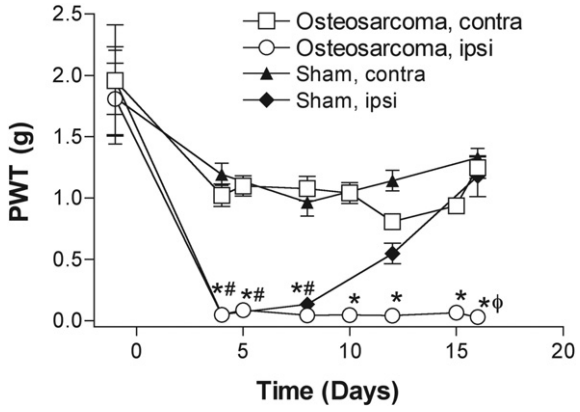

Fig. 2. Tactile thresholds for sham and osteosarcoma mice (injected with 10^5 cells into the medullary space) over time. Each time point represents mean±SEM, n=5–9 mice per group. $P<0.05$ is indicated by * comparing osteosarcoma, ipsilateral to osteosarcoma, contralateral, # comparing sham ipsilateral to sham contralateral and ϕ comparing osteosarcoma ipsilateral to sham ipsilateral.

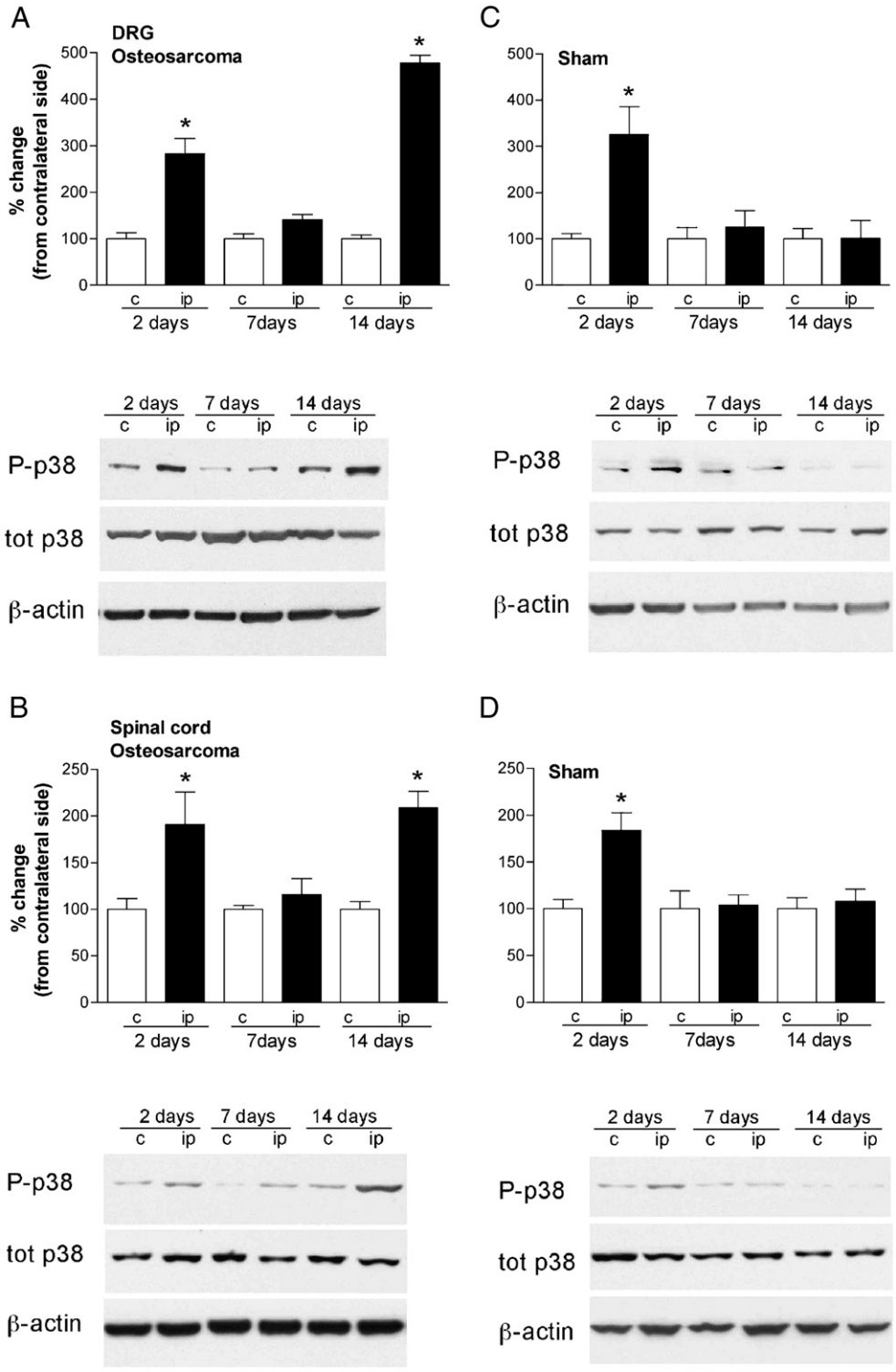

Fig. 3. Phosphorylation of p38 in DRG and spinal cord 2, 7 and 14 days after injection of osteosarcoma cells to the femur. Bar graphs showing % change in phospho-p38 (P-p38) immunoreactivity normalized to b-actin in ipsilateral (tumor-bearing) side as compared to contralateral side in osteosarcoma (A) DRG and (B) spinal samples and sham (C) DRG and (D) spinal samples. These data represents mean±SEM, $n=4$ mice per group. Representative western blots for P-p38, total p38 (tot p38) or β-actin for osteosarcoma DRG spinal samples and sham DRG and spinal samples are shown below each respective bar graph. * indicates $P<0.05$ as compared to respective contralateral tissue.

the ipsilateral DRG p38 positive neurons and very few neurons were found positive for P-p38 immunoreactivity on the contralateral side.

In the spinal cord a very distinct pattern of P-p38-posititive cells was observed in the superficial lamina of the ipsilateral dorsal horn (Fig. 5a). No such p38 activation was detected in spinal cords from sham mice (Fig. 5b). Colocalization with the neuronal marker Neuronal N showed that the p38 immunoreactive cells were a subpopulation of dorsal horn neurons (Fig. 5c, d). While the majority of p38 immunopositive cells colocalized with the neuronal marker, a few cells were detected that did not overlap with this marker (arrowhead, Fig. 5d). Also, there was weak p38 immunoreactivity in glia-like cells throughout the gray matter; however, there were no

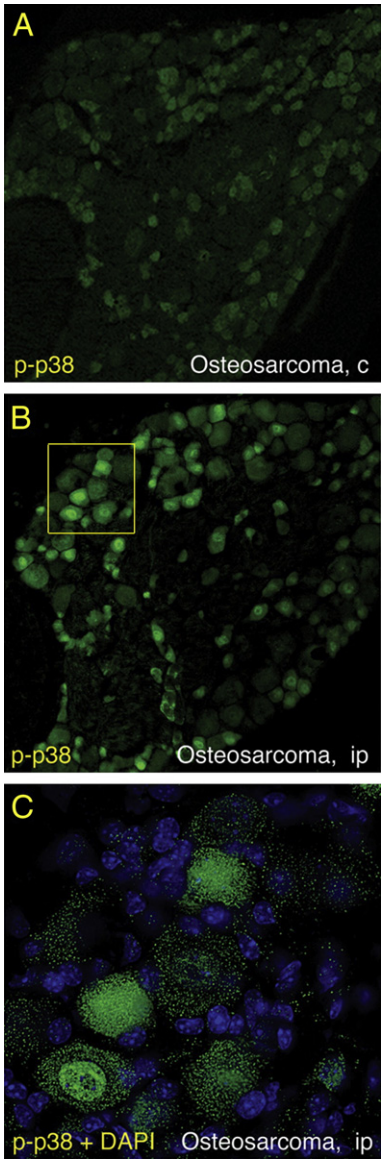

Fig. 4. Images showing ipsilateral and contralateral DRG sections from osteosarcoma mice 14 days after surgery immunolabeled for P-p38 (green). An increase in phosphorylated-p38 (p-p38) signal was observed by confocal microscopy in (B) small and medium sized ipsilateral DRG neurons in comparison to (A) contralateral DRGs. (C) Close up of DRG section (square in B) stained with nuclear marker, DAPI (blue) showing that p-p38 (green) was present predominantly in nucleus but to some extent also in the cytosol.

evident differences in staining between ipsilateral and contralateral side.

3.4. Body weight and food consumption

Comparison of the daily food consumption revealed a modest drop during the days just post-surgery (Fig. 6a). Comparing the intervals −4–1, 0–4, 5–12 and 13–15 days before and after surgery, no difference was observed between the different groups and all food consumptions equaled or exceeded pre-surgery consumption and this upward trend continued in vehicle and sham groups as well as in the low and high SCIO-469 dose groups (Fig. 6c). Comparison of bodyweights over time revealed a trend in weight gain for the sham group, significant in the day 5–12 and 13–15 interval (Fig. 6d). The tumor-bearing mice remained stable around the weight measured prior to surgery (Fig. 6b) suggesting an interruption in the weight gain normally observed over the 14 days after surgery. However, there was no significant difference between vehicle and SCIO-469 dose groups.

3.5. SCIO-469 serum concentration

The p38 inhibitor SCIO-469 was supplied in chow as two concentrations, which were calculated based on daily food consumption to provide dosing equivalent to approximately 200 or 600 mg/kg/day (low and high dose). On day 15/16 i.e., at the end of the study, cardiac blood was sampled and analyzed and 7.5±2.5 μM (low dose) and 29±7 μM (high dose) of SCIO-469 was detected in plasma ($P<0.05$). Hence, a dose-dependent relationship was observed between the dose of SCIO-469 in the chow and plasma concentration of the inhibitor.

3.6. Effect of SCIO-469 on bone-cancer-induced allodynia

Addition of SCIO-469 to the chow starting 5 days post-surgery in doses estimated to be equivalent to 200 and 600 mg/kg/day (see above) had no effect on tactile allodynia in mice injected with osteosarcoma cells (Fig. 7a). Mice receiving SCIO-469 showed an improvement in the clinical score, although this reversal only reached statistical significance with the 200 mg/kg/day dosing (Fig. 7b).

3.7. Tumor-induced bone osteolysis

3.7.1. Radiographic analysis

Radiographs of anesthetized mice were obtained day 5, 13 and 16 in order to evaluate the effect of p38 inhibition on bone destruction. Sham-injected mice did not demonstrate significant bone destruction at any time point as assessed by scoring of the radiographs (Fig. 8a, b). In the vehicle treated osteosarcoma mice extensive bone loss was observed day 13 and 16 (2.1±0.4 and 2.6±0.4 respectively) (Fig. 8a, c). Treatment of tumor-bearing mice with SCIO-469 from day 5–16 post-tumor injection did not result in a significant reduction in bone resorption (low dose, 1.4±0.4 and 2.1±0.3; high dose, 2.0±0.2, 2.2±0.3) (Fig. 8a).

3.7.2. μ-CT scan

Micro-computed tomography (μ-CT) was used to assess the changes in three-dimensional trabecular microstructure in the ipsilateral and contralateral femur. Total bone volume per tissue volume (BV/TV), connectivity density and cortical thickness were assessed (Table 2). Connectivity density is a measure for the number of trabeculae per unit volume. Cortical thickness is expressed as the average thickness of the 3D cortex across the inner and outer cortical surfaces of the specimen. No statistical significance was reached in this experiment, hence SCIO-469 did not reduce bone erosion.

3.8. Tumor-induced bone osteoclast proliferation

3.8.1. Histomorphometric analysis

Bone morphogenesis, remodeling, and resorption are controlled in part by osteoclasts. It has been reported that activation of the p38 pathway plays an important role in osteoclast differentiation and that blocking p38 activity inhibits osteoclast formation and maturation in a model of collagen induced arthritis (Matsumoto et al., 2000a,b; Nishikawa et al., 2003). The effects of p38 inhibition on osteoclast proliferation and bone destruction in mice with femoral osteosarcoma were examined 16 days post-tumor injection. The number of osteoclasts was counted along the entire intramedullary bone/marrow (or tumor) interface. No osteoclast proliferation was observed in naïve and sham operated animals ($n=5$–7) In contrast, the vehicle treated osteosarcoma group showed a significant increase in number of osteoclasts along the bone/tumor interface (41.0±7.7, $n=5$). Treatment of sarcoma injected mice with the p38 inhibitor, starting 5 days after surgery, showed a tendency to reduction of number of osteoclasts along the femur (29.6±3.6, $n=7$), however, these data did not reach statistical significance, hence, p38 inhibition did not alter osteoclast proliferation.

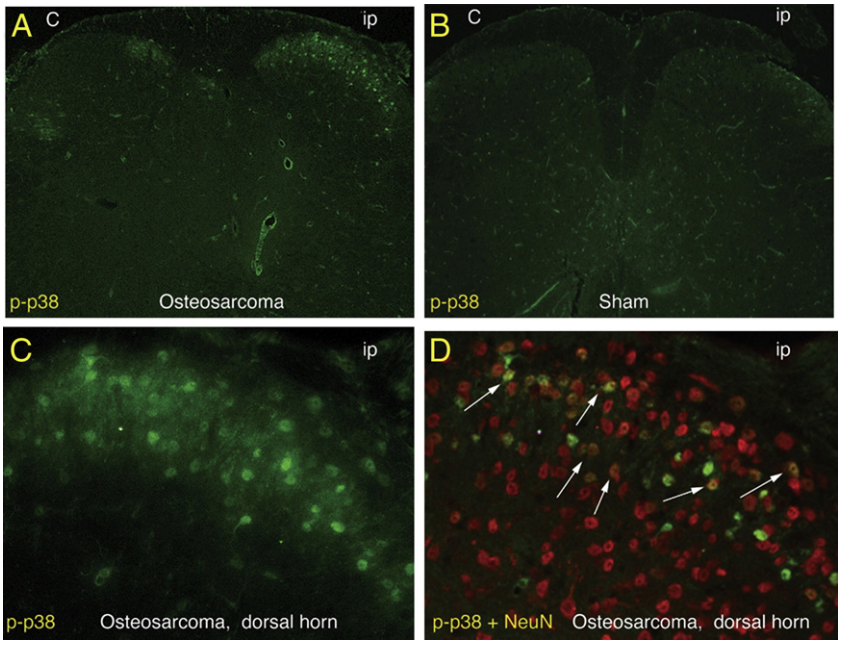

Fig. 5. Spinal cord sections from osteosarcoma and sham mice 14 days after surgery, immunostained for phosphorylated p38 (p-p38) (green) and Neuronal N (red). (A) Activated p-p38 was detected in superficial ipsilateral dorsal horn of osteosarcoma mice while (B) no ipsilateral/contralateral difference was observed in sham mice. (C) Close up of the ipsilateral dorsal horn shown in (A). Micrographs showing that the phosphorylated p38 (green) colocalized with neurons (red) in laminae I–II dorsal horn neurons (indicated with white arrows). A few cells were detected that did not co-localize with Neuronal N (indicated with arrowheads). (For interpretation of the references to colour in this figure legend, the reader is referred to the web version of this article.)

3.9. Effect of p38 inhibition on histopathology

The effects of p38 inhibition on tumor growth were examined 16 days after injection of osteosarcoma cells. Femurs were harvested day 14–16, decalcified and H&E stained. The sham mice showed a normal bone structure with darkly stained bone marrow cells and an intact trabecular system (Fig. 9b). In femurs of the vehicle treated sarcoma mice, as well as in the SCIO-469 treated tumor-bearing mice,

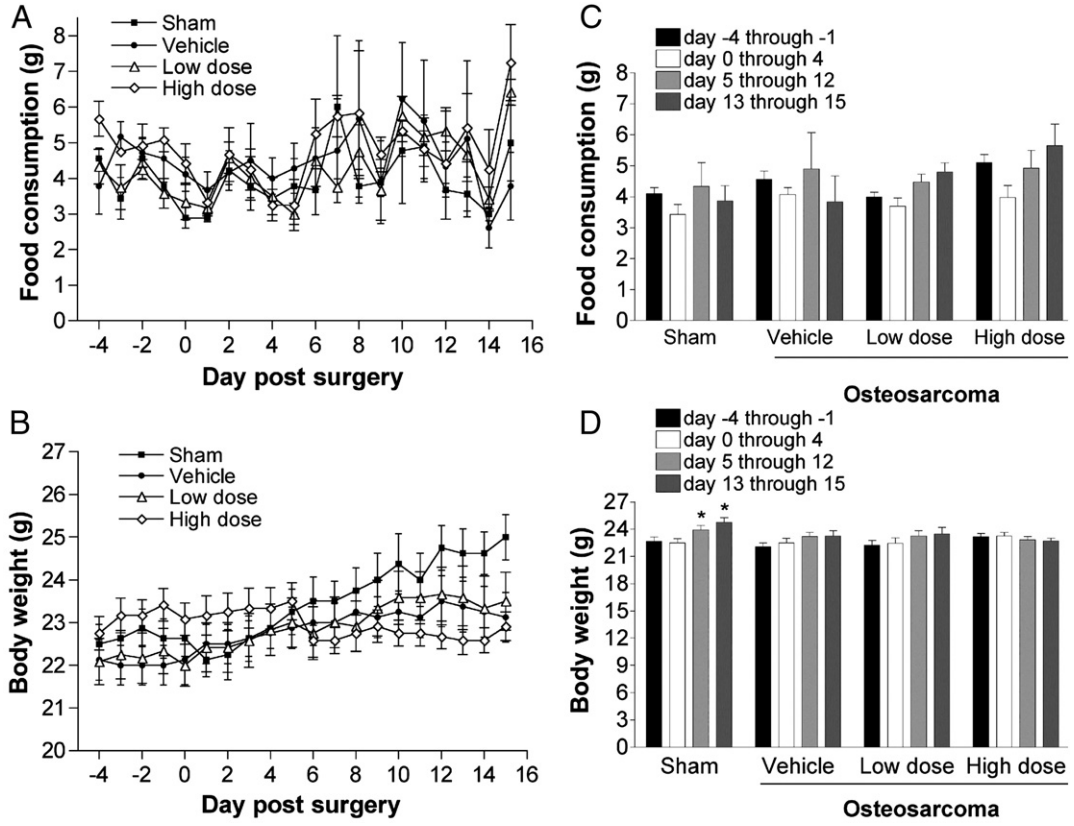

Fig. 6. Graphs depicting food consumption and body weight plotted versus time. (A, B) Food consumption and body weight was assessed every day and (C, D) average body weights and food consumption were calculated over 4 intervals; day −4 to −1 (pre-osteosarcoma); day 0–4 (post-osteosarcoma/pre-drug); day 5–12 (early post-treatment) and 13–15 (late post-treatment). Each bar and time point represents mean ± SEM. * indicates $P<0.05$ as compared to the −4 to −1 interval.

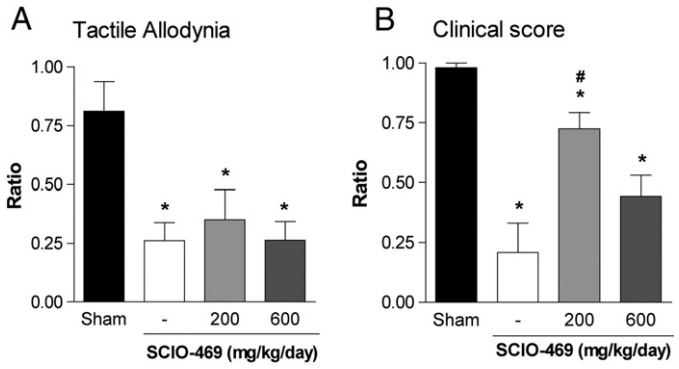

Fig. 7. Effect of SCIO-469 on tactile allodynia and clinical score. Bar graphs depicting the ratio of the baseline tactile allodynia (A) and clinical score (B) to the tactile allodynia and clinical score assessed 15 days post-surgery. Each time point and bar represents mean ± SEM, $n=8–17$ mice per group. * indicates a significant difference as compared to sham animals and # indicates a significant difference from the vehicle group.

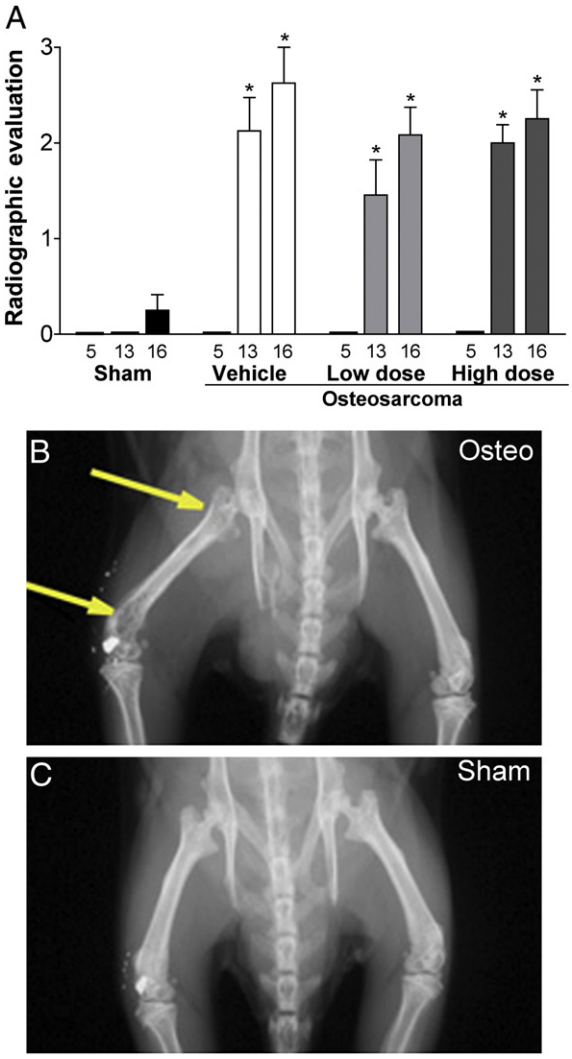

Fig. 8. Effect of p38 inhibition on osteolysis. (A) Radiographic analysis. Radiographs of anesthetized mice were obtained on day 5, 13 and 16. The extent of tumor induced femoral bone destruction was assessed by blinded observers using a 0–3 scale; (0) was given in normal bone, (1) if there was mild or up to 25% lysis of the affected bone, (2) if there was apparent or up to 50% lysis of the affected bone or (3) if there was greater than 50% lysis or complete fracture of the bone. Each bar represents mean ± SEM, $n=8–12$ mice per group. Representative radiograph of sham (B) osteosarcoma (C) mice. Arrows indicate areas of osteolysis in osteosarcoma mice that was not observed in sham mice. Local radioopacity in the distal femur indicates dental amalgam plug.

Table 2
Analysis of the three-dimensional trabecular microstructure of femurs by micro-computed tomography (μ-CT) imaging

	BV/TV	Connectivity Density [1/mm^3]	Thickness [mm]
Sham ($n=3$)	0.756+0.05	4.19+2.1	0.366+0.04
Vehicle ($n=4$)	0.640+0.06	12.75+10	0.330+0.04
Low Dose ($n=4$)	0.713+0.02	2.91+0.47	0.340+0.01
High Dose ($n=4$)	0.729+0.03	3.33+1.37	0.338+0.01

the marrow cells were replaced with more lightly stained sarcoma cells (Fig. 9c,d). In approximately 95% of the 10^5 tumor-bearing mice the presence of osteosarcoma cells had induced bone defects resulting in local fractures and extrafemoral migration of tumor cells and the histological appearance of such changes is shown in Fig. 9d. Tumor mass and intramedullary space of the femurs were measured and expressed as percentage of intramedullary space occupied by tumor (Fig. 9a). Tumor mass was found in the intramedullary space in all osteosarcoma injected mice and there was no difference between vehicle and SCIO-469 treated animals.

4. Discussion

4.1. Osteosarcoma and nociception

The present study comprises several important observations. First, a relationship between the number of osteosarcoma cell injected into the femur and the degree of developing hypersensitivity was observed. With the higher number of cells a more pronounced allodynia and impairment in the clinical score was recorded. This finding indicates that the level of tumor burden and osteolysis are important for the generation of bone cancer related pain. Second, at time points when there was a clear dissociation in allodynia between the osteosarcoma and sham group, there was an increase in p38 phosphorylation in DRG and spinal dorsal horn neurons. As p38 has been suggested to play a role in a number of different types of pain this finding led to the hypothesis that p38 also participate in the regulation of bone cancer pain.

4.2. Mechanisms of osteosarcoma-induced nociception

There are a number of factors that can contribute to the development of allodynia in conditions like osteosarcoma. i) Periosteum, mineralized bone and bone marrow are highly innervated by Aβ, Aδ and C fibers (Mach et al., 2002), all of which conduct sensory input form the bone to the spinal cord. Osteoclasts destroy bone by forming an acidic environment and the elevated H^+ ion concentrations may activate TRPV1 receptors on small primary afferents. It has been demonstrated that blocking the activation of TRPV1 receptors reduces both spontaneous and evoked pain behavior in this model (Ghilardi et al., 2005; Niiyama et al., 2007). ii) Excessive osteoclastic activity over an extended period of time will lead to loss of mechanical strength and stability of the bone. Normally silent mechanoreceptors may now be activated by the mechanical stress resulting from destabilization of the bone structure. Moreover, as the tumor continuous to grow, sensory neurons that innervate the marrow may be compressed and damaged, potentially driving nerve-injury related pain mechanisms. iii) It is appreciated that growth factors such as transforming growth factor β and NGF is released from the bone during the process of osteolysis and these factors can facilitate terminal sensitivity and directly excite sensory fibers (Grills and Schuijers, 1998; Halvorson et al., 2005). iv) Apart from the change in osteoclastic activity the tumor cells themselves express high levels proteins such as COX-2 (Sabino et al., 2002) and it is likely that secretion of prostaglandins will sensitize local nerve terminals. v) The tumor mass is often highly infiltrated with macrophages that can produce factors

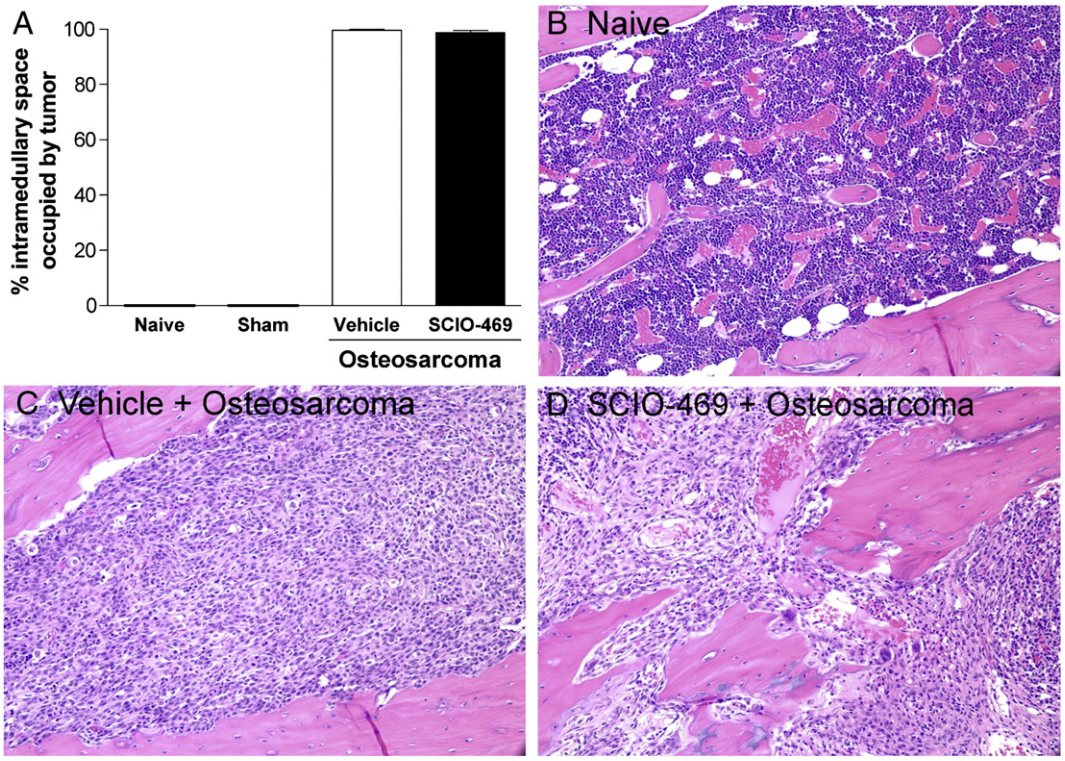

Fig. 9. Effect of p38 inhibition on tumor growth. Femurs were harvested day 15/16, decalcified and H&E stained. (A) Tumor mass and intramedullary space of the femurs were measured and expressed as percentage of intramedullary space occupied by tumor. Tumor mass was found in the intramedullary space in all osteosarcoma injected mice and there was no difference between vehicle and SCIO-469 treated animals. Each bar represents mean ± SEM, $n = 8–12$ mice per group. H&E stain of (B) normal and (C,D) sarcoma-bearing femurs, showing replacement of the darkly stained marrow cells with more lightly stained sarcoma cells that have induced bone defects resulting in local fractures and extrafemoral migration of tumor cells.

such as TNF-α and IL-β, which excite primary afferent neurons (Safieh-Garabedian et al., 1995; Sorkin et al., 1997). The different mechanisms described above are likely to lead to persistent release of neurotransmitters and proinflammatory factors at the spinal level, giving rise to spinal sensitization and facilitation of central pain processing.

4.3. Role of spinal p38

The rational for this study was based on work reporting that p38 plays important roles in processes associated with both bone cancer and pain. For example, p38 has been indicated as a positive regulator of osteoclastic activity (Matsumoto et al., 2000a,b; Lee et al., 2002; Karsdal et al., 2003; Zwerina et al., 2006b) and important in the process of formation of bone metastasis (Matsumoto et al., 2000a; Selvamurugan et al., 2002; Suarez-Cuervo et al., 2004; Zwerina et al., 2006b) as well as tumor growth [for review see (Schultz, 2003)]. In addition, p38 have repeatedly been reported activated in DRGs and spinal neuronal and non-neuronal cells in response to different types of peripheral painful injuries. Inhibition of p38 attenuate pain states of both inflammatory (Ji et al., 2002; Svensson et al., 2003b) and neuropathic (Jin et al., 2003; Schafers et al., 2003; Obata et al., 2004; Tsuda et al., 2004) nature. These properties, taken together, make p38 an interesting target for prevention of bone cancer-induced hypersensitivity and bone erosion. Notably, there is evidence for p38 being involved in several of the processes described above e.g. regulation of TRPV1 (Ji et al., 2002, Sweitzer et al., 2004) and COX-2 protein expression (Guan et al., 1997; Hwang et al., 1997), cytokine production [for review see (Adams et al., 2001)] and osteoclast differentiation (Matsumoto et al., 2000b). In addition, it has previously been demonstrated that p38 regulates calcium dependent phospholipase activity and PGE2 formation (Kramer et al., 1996; Borsch-Haubold et al., 1999; Lucas et al., 2005). It has also been shown that tumor necrosis factor alpha enhances tetrodotoxin-resistent sodium channel currents in a p38 dependent fashion, indicating that p38 may participate in modulating nociceptors excitability (Jin and Gereau, 2006).

In this work, although the p38 inhibitor SCIO-469, administrated through chow, was well tolerated and gave rise to a dose-dependent serum concentration, p38 inhibition had no effect on bone cancer-induced allodynia. The only indication of p38 contributing to bone cancer-mediated discomfort was observed in the clinical score. Mice receiving the low dose p38 containing food showed an improvement in osteosarcoma-induced ambulation impairment. In addition to nociceptive parameters, the effect of p38 inhibition on tumor burden and bone erosion was also examined. Continuous treatment with p38 inhibitor had no effect on tumor growth or osteolysis.

4.4. Spinal non-neuronal cells and osteosarcoma

An interesting feature in the bone cancer model is the observation that non-neuronal cells in the spinal cord show signs of activation. It has become increasingly appreciated that these cells contribute to spinal sensitization. Increased expression of markers used for detection of astrocyte and microglia activity has been reported both in mice (Schwei et al., 1999; Vit et al., 2006) and rats (Zhang et al., 2005) after injection of cancer cells to the femur. In a recent report it was demonstrated, in accordance with our study, that phosphorylation of p38 is increased in the spinal cord in mice with osteosarcoma (Vit et al., 2006). However the localization of p38 activation is somewhat different, while we observed phosphorylated p38 predominantly in neurons in the superficial lamina of the spinal cord, Vit et al. found an increase of activated p38 in microglia. It should be noted that we did observed weak immunoreactivity for phosphorylated p38 in spinal microglia, but no difference could be detected between the ipsilateral and contralateral side. It is possible that injection of osteosarcoma cells to the femur result in a bilateral activation of microglia. In addition, the time point for P-p38 assessment is different in the two studies.

4.5. Time course of nociception after osteosarcoma

In the early phase after surgery, tactile allodynia was observed in both the sham group and the osteosarcoma-injected mice. To our knowledge, no time course for tactile allodynia has been reported for either sham or osteosarcoma mice, whereas many studies have demonstrated a separation between sham and tumor-bearing mice at later time points (Schwei et al., 1999; Honore et al., 2000; Ghilardi et al., 2005; Vit et al., 2006). The early phase allodynia observed in both sham and osteosarcoma injected mice is likely a result of the bone trauma associated with drilling trough the condoyle to make access to the intramedullary space. Based on the biphasic profile of phosphorylation of p38 in the DRGs and spinal cord p38 could potentially contribute to both phases of pain. The level of p38 phosphorylation was increased the ipsilateral side, as compared to the contralateral side 2 days after surgery but lower, and not different between the two sides, day 7. If p38 is a mediator of "post-surgical and post-bone trauma" pain, these data would suggest that p38 is activated during induction but not the same extent during maintenance of this type of pain. However, due to the design of this study (no drug administration to the sham group and introduction of SCIO-469 on day 5 and assessment of allodynia day 15 and 16) no conclusions can be made with regards to the effect of p38 inhibition on post-surgical or "post-bone trauma" pain.

4.6. Issues relating to the effects of the p38 inhibitor

The p38 inhibitor employed in these studies was delivered through the chow. This approach has significant benefits as it reduced the need for restraint, which is required for oral intubations. This is of particular importance as the osteosarcoma femur becomes extremely weak due to osteolysis and such handling would lead to a greatly increased fracture rate requiring sacrifice. To administer the drug in the chow also provides a more even delivery over time. Mice tend to have their highest consumption in the nocturnal cycle and this could potentially lead to fluctuation in plasma concentration over the day, however, this drug delivery paradigm was still considered to be superior as compared to oral gavages. The plasma concentration of SCIO-469 was measured in blood drawn just after the last behavioral testing and sufficiently high drug concentrations were measured. Importantly, the different doses used for this study lead to plasma levels proportional to the dosing as assessed at the end of the study. However, a *caveat* is that this administration system is only appropriate as long as animals continue to feed. In pilot work it was observed that there is a significant drop in feeding and body weight by day 15/16, and therefore the study was not allowed to continue past day 16. It would have been ideal to assess blood levels on a daily basis during the study to assure an even dosing. This was considered to be too invasive and therefore body weight and food consumption was monitored closely. Examination of these parameters revealed maintenance or increases in body weight emphasizing that adequate food consumption was maintained over the duration of the study.

Based on the findings that p38 is activated both in the peripheral and central nervous system in bone tumor-bearing mice lead us to hypothesize that p38 may be a novel target for pain relief in bone cancer-induced hypersensitivity. Surprisingly, no anti-allodynic effect could be detected after oral administration of SCIO-469. Due to the dosing regimen we cannot predict the local concentration of the drug, but serum levels were in the same range that has shown an anti-inflammatory effect in models of asthma (Nath et al., 2006). In addition, in an earlier study (Vanderkerken et al., 2007), in which SCIO-469 was mixed with the chow at doses of 150 and 450 mg/kg, a dose-dependent increase in survival and decrease in development of bone disease was observed in a mouse model of multiple myeloma. It is possible that p38 in the spinal cord plays a dominant role in the regulation of bone cancer pain and that SCIO-469 did not reach sufficient levels in the cerebrospinal fluid. Alternatively, despite activation of p38 in structures related to pain processing, this enzyme may not play a major role in bone cancer pain, or at the time points when the animals were tested, other systems may override the removal of p38 signaling.

4.7. p38 in cancer pathology

p38 has also been suggested to have a disease-modifying effect in pathologies involving bone and cartilage. In models of arthritis it has been demonstrated that inhibition of p38 reduces the number of osteoclasts and bone erosion (Nishikawa et al., 2003; Zwerina et al., 2006a). Osteoblasts are triggered by factors such as parathyroid hormone, IL-6 and PGE2 to induce osteoclast formation in a p38 dependent fashion (Matsumoto et al., 2000a,b). However, this system is tightly balanced as p38 activity in osteoblasts also drive synthesis of osteopotegrein, a decoy receptor that inhibits osteoclastogenesis (Pantouli et al., 2005). The number of osteoclasts along the intramedullary interface showed a "tendency" to reduction in the presence of p38 inhibitor, but statistical significance was not reached. In addition, whereas the role of p38 in osteoclastogenesis is well studied it is less clear if p38 activity is necessary for osteoclast function (Kumar et al., 2001; Li et al., 2002). Assessment of osteolysis by X-ray as well as with a more sensitive technique, μ-CT-scanning, did not point to a reduction in bone loss in the presence of SCIO-469. Hence, this study failed to provide evidence for p38 inhibition reducing osteolysis. In terms of tumor growth, p38 has been discussed to have both oncogenic and tumor suppressive effects [for review see (Rennefahrt et al., 2005)]. Blocking p38 activity did not reduce the tumor burden in this study indicating that p38 activity is not critical for the cell proliferation in this model of bone cancer.

4.8. Summary

In summary, we have demonstrated that p38 is activated in DRG and spinal neurons in an in vivo model of bone cancer. Introducing the p38 inhibitor SCIO-469 in the chow in a therapeutic fashion, i.e. after establishment of the disease, was sufficient to reduce spontaneous measures of bone cancer pain behaviors, but did not block evoked allodynia. The involvement of p38-mediated signaling in osteosarcoma-induced pain and bone pathology is complex and further studies are needed in order to determine the roles this kinase play in bone cancer.

Acknowledgements

This work was supported by NS07407 (TLY), NS16541 (TLY) and UCSD Cancer Center Grant (ZDL) and Scios Inc (Fermont, CA), which provided SCIO-469 and partial funding. Authors are thankful to Zeke Li and Ramoina Almirez for their technical help.

References

Adams JL, Badger AM, Kumar S, Lee JC. p38 MAP kinase: molecular target for the inhibition of pro-inflammatory cytokines. Prog Med Chem 2001;38:1–60.

Borsch-Haubold AG, Ghomashchi F, Pasquet S, Goedert M, Cohen P, Gelb MH, et al. Phosphorylation of cytosolic phospholipase A2 in platelets is mediated by multiple stress-activated protein kinase pathways. Eur J Biochem 1999;265:195–203.

Chaplan SR, Bach FW, Pogrel JW, Chung JM, Yaksh TL. Quantitative assessment of tactile allodynia in the rat paw. J Neurosci Methods 1994;53:55–63.

Coleman RE. Metastatic bone disease: clinical features, pathophysiology and treatment strategies. Cancer Treat Rev 2001;27:165–76.

Ghilardi JR, Rohrich H, Lindsay TH, Sevcik MA, Schwei MJ, Kubota K, et al. Selective blockade of the capsaicin receptor TRPV1 attenuates bone cancer pain. J Neurosci 2005;25:3126–31.

Grills BL, Schuijers JA. Immunohistochemical localization of nerve growth factor in fractured and unfractured rat bone. Acta Orthop Scand 1998;69:415–9.

Guan Z, Baier LD, Morrison AR. p38 mitogen-activated protein kinase down-regulates nitric oxide and up-regulates prostaglandin E2 biosynthesis stimulated by interleukin-1beta. J Biol Chem 1997;272:8083–9.

Halvorson KG, Kubota K, Sevcik MA, Lindsay TH, Sotillo JE, Ghilardi JR, et al. A blocking antibody to nerve growth factor attenuates skeletal pain induced by prostate tumor cells growing in bone. Cancer Res 2005;65:9426–35.

Honore P, Rogers SD, Schwei MJ, Salak-Johnson JL, Luger NM, Sabino MC, et al. Murine models of inflammatory, neuropathic and cancer pain each generates a unique set of neurochemical changes in the spinal cord and sensory neurons. Neuroscience 2000;98:585–98.
Hwang D, Jang BC, Yu G, Boudreau M. Expression of mitogen-inducible cyclooxygenase induced by lipopolysaccharide: mediation through both mitogen-activated protein kinase and NF-kappaB signaling pathways in macrophages. Biochem Pharmacol 1997;54:87–96.
Jiang Y, Zhao J, White DL, Genant HK. Micro CT and micro MR imaging of 3D architecture of animal skeleton. J Musculoskel Neuron Interact 2000;1:45–51.
Jiang Y, Zhao J, Genant HK. Macro and micro imaging of bone architecture. In: Bilezikian JP, Raisz LG, Rodan GA, editors. Principles of Bone Biology. 2nd ed. San Diego, CA: Academic Press; 2002. p. 1599–623.
Ji RR, Samad TA, Jin SX, Schmoll R, Woolf CJ. p38 MAPK activation by NGF in primary sensory neurons after inflammation increases TRPV1 levels and maintains heat hyperalgesia. Neuron 2002;36:57–68.
Jin SX, Zhuang ZY, Woolf CJ, Ji RR. p38 mitogen-activated protein kinase is activated after a spinal nerve ligation in spinal cord microglia and dorsal root ganglion neurons and contributes to the generation of neuropathic pain. J Neurosci 2003;23:4017–22.
Jin X, Gereau RWt. Acute p38-mediated modulation of tetrodotoxin-resistant sodium channels in mouse sensory neurons by tumor necrosis factor-alpha. J Neurosci 2006;26:246–55.
Karsdal MA, Hjorth P, Henriksen K, Kirkegaard T, Nielsen KL, Lou H, et al. Transforming growth factor-beta controls human osteoclastogenesis through the p38 MAPK and regulation of RANK expression. J Biol Chem 2003;278:44975–87.
Kramer RM, Roberts EF, Um SL, Borsch-Haubold AG, Watson SP, Fisher MJ, et al. p38 mitogen-activated protein kinase phosphorylates cytosolic phospholipase A2 (cPLA2) in thrombin-stimulated platelets. Evidence that proline-directed phosphorylation is not required for mobilization of arachidonic acid by cPLA2. J Biol Chem 1996;271:27723–9.
Kumar S, Votta BJ, Rieman DJ, Badger AM, Gowen M, Lee JC. IL-1- and TNF-induced bone resorption is mediated by p38 mitogen activated protein kinase. J Cell Physiol 2001;187:294–303.
Lee SE, Woo KM, Kim SY, Kim HM, Kwack K, Lee ZH, et al. The phosphatidylinositol 3-kinase, p38, and extracellular signal-regulated kinase pathways are involved in osteoclast differentiation. Bone 2002;30:71–7.
Li X, Udagawa N, Itoh K, Suda K, Murase Y, Nishihara T, et al. p38 MAPK-mediated signals are required for inducing osteoclast differentiation but not for osteoclast function. Endocrinology 2002;143:3105–13.
Lucas KK, Svensson CI, Hua XY, Yaksh TL, Dennis EA. Spinal phospholipase A2 in inflammatory hyperalgesia: role of group IVA cPLA2. Br J Pharmacol 2005;144:940–52.
Luger NM, Mach DB, Sevcik MA, Mantyh PW. Bone cancer pain: from model to mechanism to therapy. J Pain Symptom Manage 2005;29:S32–46.
Mach DB, Rogers SD, Sabino MC, Luger NM, Schwei MJ, Pomonis JD, et al. Origins of skeletal pain: sensory and sympathetic innervation of the mouse femur. Neuroscience 2002;113:155–66.
Matsumoto M, Sudo T, Maruyama M, Osada H, Tsujimoto M. Activation of p38 mitogen-activated protein kinase is crucial in osteoclastogenesis induced by tumor necrosis factor. FEBS Lett 2000a;486:23–8.
Matsumoto M, Sudo T, Saito T, Osada H, Tsujimoto M. Involvement of p38 mitogen-activated protein kinase signaling pathway in osteoclastogenesis mediated by receptor activator of NF-kappa B ligand (RANKL). J Biol Chem 2000b;275:31155–61.
Medicherla S, Ma JY, Mangadu R, Jiang Y, Zhao JJ, Almirez R, et al. A selective p38 mitogen-activated protein kinase inhibitor reverses cartilage and bone destruction in mice with collagen-induced arthritis. J Pharmacol Exp Ther 2006;318:132–41.
Nath P, Leung SY, Williams A, Noble A, Chakravarty SD, Luedtke GR, et al. Importance of p38 mitogen-activated protein kinase pathway in allergic airway remodelling and bronchial hyperresponsiveness. Eur J Pharmacol. 2006;544(1–3):160–7.
Niiyama Y, Kawamata T, Yamamoto J, Omote K, Namiki A. Bone cancer increases transient receptor potential vanilloid subfamily 1 expression within distinct subpopulations of dorsal root ganglion neurons. Neuroscience 2007.
Nishikawa M, Myoui A, Tomita T, Takahi K, Nampei A, Yoshikawa H. Prevention of the onset and progression of collagen-induced arthritis in rats by the potent p38 mitogen-activated protein kinase inhibitor FR167653. Arthritis Rheum 2003;48:2670–81.
Obata K, Yamanaka H, Kobayashi K, Dai Y, Mizushima T, Katsura H, et al. Role of mitogen-activated protein kinase activation in injured and intact primary afferent neurons for mechanical and heat hypersensitivity after spinal nerve ligation. J Neurosci 2004;24:10211–22.
Ono K, Han J. The p38 signal transduction pathway: activation and function. Cell Signal 2000;12:1–13.
Pantouli E, Boehm MM, Koka S. Inflammatory cytokines activate p38 MAPK to induce osteoprotegerin synthesis by MG-63 cells. Biochem Biophys Res Commun 2005;329:224–9.
Parfitt AM, Mathews CH, Villanueva AR, Kleerekoper M, Frame B, Rao DS. Relationships between surface, volume, and thickness of iliac trabecular bone in aging and in osteoporosis. Implications for the microanatomic and cellular mechanisms of bone loss. J Clin Invest 1983;72:1396–409.
Portenoy RK, Payne D, Jacobsen P. Breakthrough pain: characteristics and impact in patients with cancer pain. Pain 1999;81:129–34.
Rennefahrt U, Janakiraman M, Ollinger R, Troppmair J. Stress kinase signaling in cancer: fact or fiction? Cancer Lett 2005;217:1–9.
Sabino MA, Ghilardi JR, Jongen JL, Keyser CP, Luger NM, Mach DB, et al. Simultaneous reduction in cancer pain, bone destruction, and tumor growth by selective inhibition of cyclooxygenase-2. Cancer Res 2002;62:7343–9.
Safieh-Garabedian B, Poole S, Allchorne A, Winter J, Woolf CJ. Contribution of interleukin-1 beta to the inflammation-induced increase in nerve growth factor levels and inflammatory hyperalgesia. Br J Pharmacol 1995;115:1265–75.
Schafers M, Svensson CI, Sommer C, Sorkin LS. Tumor necrosis factor-alpha induces mechanical allodynia after spinal nerve ligation by activation of p38 MAPK in primary sensory neurons. J Neurosci 2003;23:2517–21.
Scholz J, Woolf CJ. Can we conquer pain? Nat Neurosci 2002;5(Suppl):1062–7.
Schultz RM. Potential of p38 MAP kinase inhibitors in the treatment of cancer. Prog Drug Res 2003;60:59–92.
Schwei MJ, Honore P, Rogers SD, Salak-Johnson JL, Finke MP, Ramnaraine ML, et al. Neurochemical and cellular reorganization of the spinal cord in a murine model of bone cancer pain. J Neurosci 1999;19:10886–97.
Selvamurugan N, Fung Z, Partridge NC. Transcriptional activation of collagenase-3 by transforming growth factor-beta1 is via MAPK and Smad pathways in human breast cancer cells. FEBS Lett 2002;532:31–5.
Sorkin LS, Xiao WH, Wagner R, Myers RR. Tumour necrosis factor-alpha induces ectopic activity in nociceptive primary afferent fibres. Neuroscience 1997;81:255–62.
Suarez-Cuervo C, Merrell MA, Watson L, Harris KW, Rosenthal EL, Vaananen HK, et al. Breast cancer cells with inhibition of p38alpha have decreased MMP-9 activity and exhibit decreased bone metastasis in mice. Clin Exp Metastasis 2004;21:525–33.
Svensson CI, Hua XY, Protter AA, Powell HC, Yaksh TL. Spinal p38 MAP kinase is necessary for NMDA-induced spinal PGE(2) release and thermal hyperalgesia. Neuroreport 2003a;14:1153–7.
Svensson CI, Marsala M, Westerlund A, Calcutt NA, Campana WM, Freshwater JD, et al. Activation of p38 mitogen-activated protein kinase in spinal microglia is a critical link in inflammation-induced spinal pain processing. J Neurochem 2003b;86:1534–44.
Sweitzer SM, Peters MC, Ma JY, Kerr I, Mangadu R, Chakravarty S, et al. Peripheral and central p38 MAPK mediates capsaicin-induced hyperalgesia. Pain 2004;3:278–85.
Takeshita S, Namba N, Zhao J, Jiang Y, Genant HK, Silva MJ, et al. SHIP-deficient mice are severely osteoporotic due to increased numbers of hyper-resorptive osteoclasts. Nat Med 2002;8:943–9.
Tsuda M, Mizokoshi A, Shigemoto-Mogami Y, Koizumi S, Inoue K. Activation of p38 mitogen-activated protein kinase in spinal hyperactive microglia contributes to pain hypersensitivity following peripheral nerve injury. Glia 2004;45:89–95.
Vit JP, Ohara PT, Tien DA, Fike JR, Eikmeier L, Beitz A, et al. The analgesic effect of low dose focal irradiation in a mouse model of bone cancer is associated with spinal changes in neuro-mediators of nociception. Pain 2006;120:188–201.
Vanderkerken K, Medicherla S, Coulton L, Menu E, Protter AA, Higgins LS, et al. Inhibition of p38 MAPK prevents the development of myeloma bone disease, reduces tumor burden and increases survival in murine models of myeloma. Cancer Res 2007;67:4572–7.
Widmann C, Gibson S, Jarpe MB, Johnson GL. Mitogen-activated protein kinase: conservation of a three-kinase module from yeast to human. Physiol Rev 1999;79:143–80.
Woolf CJ, Salter MW. Neuronal plasticity: increasing the gain in pain. Science 2000;288:1765–9.
Yoneda T. Cellular and molecular mechanisms of breast and prostate cancer metastasis to bone. Eur J Cancer 1998;34:240–5.
Zhang RX, Liu B, Wang L, Ren K, Qiao JT, Berman BM, et al. Spinal glial activation in a new rat model of bone cancer pain produced by prostate cancer cell inoculation of the tibia. Pain 2005;118:125–36.
Zwerina J, Hayer S, Redlich K, Bobacz K, Kollias G, Smolen JS, et al. Activation of p38 MAPK is a key step in tumor necrosis factor-mediated inflammatory bone destruction. Arthritis Rheum 2006a;54:463–72.
Zwerina J, Hayer S, Redlich K, Bobacz K, Kollias G, Smolen JS, et al. Activation of p38 MAPK is a key step in tumor necrosis factor-mediated inflammatory bone destruction. Arthritis Rheum 2006b;54:463–72.